Concept for power scaling second harmonic generation using a cascade of nonlinear crystals

A. K. Hansen,[1,*] M. Tawfieq,[1] O. B. Jensen,[1] P. E. Andersen,[1] B. Sumpf,[2] G. Erbert,[2] and P. M. Petersen[1]

[1]*Department of Photonics Engineering, Technical University of Denmark, 4000 Roskilde, Denmark*
[2]*Ferdinand-Braun-Institut für Höchstfrequenztechnik, Gustav-Kirchhoff-Straße 4, 12489 Berlin, Germany*
[*]*ankrh@fotonik.dtu.dk*

Abstract: Within the field of high-power second harmonic generation (SHG), power scaling is often hindered by adverse crystal effects such as thermal dephasing arising from the second harmonic (SH) light, which imposes limits on the power that can be generated in many crystals. Here we demonstrate a concept for efficient power scaling of single-pass SHG beyond such limits using a cascade of nonlinear crystals, in which the first crystal is chosen for high nonlinear efficiency and the subsequent crystal(s) are chosen for power handling ability. Using this highly efficient single-pass concept, we generate 3.7 W of continuous-wave diffraction-limited $(M^2 = 1.25)$ light at 532 nm from 9.5 W of non-diffraction-limited $(M^2 = 7.7)$ light from a tapered laser diode, while avoiding significant thermal effects. Besides constituting the highest SH power yet achieved using a laser diode, this demonstrates that the concept successfully combines the high efficiency of the first stage with the good power handling properties of the subsequent stages. The concept is generally applicable and can be expanded with more stages to obtain even higher efficiency, and extends also to other combinations of nonlinear media suitable for other wavelengths.

OCIS codes: (140.2020) Diode lasers; (160.3730) Lithium niobate; (160.4330) Nonlinear optical materials; (190.2620) Harmonic generation and mixing; (190.4360) Nonlinear optics, devices; (190.4870) Photothermal effects.

References and links

1. D. N. Nikogosyan, *Nonlinear Optical Crystals: A Complete Survey* (Springer Science, 2005).
2. N. B. Angert, V. M. Garmash, N. I. Pavlova, and A. V. Tarasov, "Influence of color centers on the optical properties of KTP crystals and on the efficiency of the laser radiation frequency conversion in these crystals," Sov. J. Quantum Electron. **21**(4), 426–428 (1991).
3. Z. M. Liao, S. A. Payne, J. Dawson, A. Drobshoff, C. Ebbers, D. Pennington, and L. Taylor, "Thermally induced dephasing in periodically poled KTP frequency-doubling crystals," J. Opt. Soc. Am. B **21**(12), 2191 (2004).
4. G. Li, Y. Cui, and J. Wang, "Photorefractive inhibition of second harmonic generation in periodically poled MgO doped $LiNbO_3$ waveguide," Opt. Express **21**(19), 21790–21799 (2013).
5. F. J. Kontur, I. Dajani, Y. Lu, and R. J. Knize, "Frequency-doubling of a CW fiber laser using PPKTP, PPMgSLT, and PPMgLN," Opt. Express **15**(20), 12882–12889 (2007).
6. O. A. Louchev, N. E. Yu, S. Kurimura, and K. Kitamura, "Thermal inhibition of high-power second-harmonic generation in periodically poled $LiNbO_3$ and $LiTaO_3$ crystals," Appl. Phys. Lett. **87**(13), 131101 (2005).
7. H. H. Lim, T. Katagai, S. Kurimura, T. Shimizu, K. Noguchi, N. Ohmae, N. Mio, and I. Shoji, "Thermal performance in high power SHG characterized by phase-matched calorimetry," Opt. Express **19**(23), 22588–22593 (2011).
8. S. Sinha, D. S. Hum, K. E. Urbanek, Y. Lee, M. J. F. Digonnet, M. M. Fejer, and R. L. Byer, "Room-temperature stable generation of 19 watts of single-frequency 532-nm radiation in a periodically poled lithium tantalate crystal," J. Lightwave Technol. **26**(24), 3866–3871 (2008).
9. S. V. Tovstonog, S. Kurimura, I. Suzuki, K. Takeno, S. Moriwaki, N. Ohmae, N. Mio, and T. Katagai, "Thermal effects in high-power CW second harmonic generation in Mg-doped stoichiometric lithium tantalate," Opt. Express **16**(15), 11294–11299 (2008).
10. D. Fluck and P. Günter, "Efficient second-harmonic generation by lens wave-guiding in $KNbO_3$ crystals," Opt. Commun. **147**(4-6), 305–308 (1998).

#239674 - $15.00 USD Received 24 Apr 2015; revised 29 May 2015; accepted 31 May 2015; published 8 Jun 2015

11. S. C. Kumar, G. K. Samanta, K. Devi, and M. Ebrahim-Zadeh, "High-efficiency, multicrystal, single-pass, continuous-wave second harmonic generation," Opt. Express **19**(12), 11152–11169 (2011).
12. R. Thompson, M. Tu, D. Aveline, N. Lundblad, and L. Maleki, "High power single frequency 780nm laser source generated from frequency doubling of a seeded fiber amplifier in a cascade of PPLN crystals," Opt. Express **11**(14), 1709–1713 (2003).
13. S. Guo, J. Wang, Y. Han, and J. He, "Frequency doubling of cw 1560nm laser with single-pass, double-pass and cascaded MgO:PPLN crystals and frequency locking to Rb D_2 line," Proc. SPIE **8772**, 87721B (2013).
14. S. Vasilyev, A. Nevsky, I. Ernsting, M. Hansen, J. Shen, and S. Schiller, "Compact all-solid-state continuous-wave single-frequency UV source with frequency stabilization for laser cooling of Be^+ ions," Appl. Phys. B **103**(1), 27–33 (2011).
15. B. Sumpf, K.-H. Hasler, P. Adamiec, F. Bugge, F. Dittmar, J. Fricke, H. Wenzel, M. Zorn, G. Erbert, and G. Tränkle, "High-brightness quantum well tapered lasers," IEEE J. Sel. Top. Quantum Electron. **15**(3), 1009–1020 (2009).
16. O. B. Jensen, P. E. Andersen, B. Sumpf, K.-H. Hasler, G. Erbert, and P. M. Petersen, "1.5 W green light generation by single-pass second harmonic generation of a single-frequency tapered diode laser," Opt. Express **17**(8), 6532–6539 (2009).
17. C. Fiebig, S. Pekarek, K. Paschke, M. Uebernickel, T. Südmeyer, U. Keller, and G. Erbert, "High-brightness distributed-bragg-reflector tapered diode lasers: pushing your application to the next level," Proc. SPIE **7918**, 79180R (2011).
18. O. B. Jensen, A. K. Hansen, A. Muller, B. Sumpf, A. Unterhuber, W. Drexler, P. M. Petersen, and P. E. Andersen, "Power scaling of nonlinear frequency converted tapered diode lasers for biophotonics," IEEE J. Sel. Top. Quantum Electron. **20**(2), 307–321 (2014).
19. T. Meyer, M. Schmitt, B. Dietzek, and J. Popp, "Accumulating advantages, reducing limitations: Multimodal nonlinear imaging in biomedical sciences - the synergy of multiple contrast mechanisms," J. Biophotonics **6**(11-12), 887–904 (2013).
20. T. Kamali, B. Považay, S. Kumar, Y. Silberberg, B. Hermann, R. Werkmeister, W. Drexler, and A. Unterhuber, "Hybrid single-source online Fourier transform coherent anti-Stokes Raman scattering/optical coherence tomography," Opt. Lett. **39**(19), 5709–5712 (2014).
21. G. D. Boyd and D. A. Kleinman, "Parametric interaction of focused Gaussian light beams," J. Appl. Phys. **39**(8), 3597 (1968).
22. S. G. Sabouri, C. K. Suddapalli, A. Khorsandi, and M. Ebrahim-Zadeh, "Focusing optimization for high-power continuous-wave second-harmonic generation in the presence of thermal effects," IEEE J. Sel. Top. Quantum Electron. **21**(1), 185–192 (2015).
23. A. G. Schott, "Optical Glass Data Sheets," http://www.schott.com/advanced_optics/english/download/schott-optical-glass-collection-datasheets-april-2015-eng.pdf.
24. T. Kasamatsu, H. Kubomura, and H. Kan, "Numerical simulation of conversion efficiency and beam quality factor in second harmonic generation with diffraction and pump depletion," Jpn. J. Appl. Phys. **44**(12), 8495–8497 (2005).

1. Introduction

The challenge of achieving high conversion efficiency in frequency doubling (second harmonic generation, SHG) of continuous wave laser beams is one of high importance for many applications and has attracted attention since the 1960s with the discovery of the laser. Single-pass SHG in particular is simple, compact, alignment insensitive and is generally well suited to integration in larger systems.

Nonlinear materials exist for frequency doubling into many wavelengths throughout the visible region as well as into both the ultraviolet and infrared spectral regions [1]. However, not all nonlinear media are suited for high powers of the second harmonic (SH) because of adverse effects such as photochromism [2,3], photorefractivity [4] or thermal dephasing due to absorption [3,5,6].

For this reason, the choice of crystal for an SHG setup is often determined by the required output power, with higher powers requiring better power handling ability of the crystal. It is well documented in the literature [5,6] that one of the most efficient crystals in current widespread use, periodically poled MgO-doped congruent lithium niobate (PPMgCLN), is in general not suitable for generating more than 2-3 W of light in the green spectral region due to thermal dephasing and thermal lensing caused by SH absorption. Alternative crystal materials with better power handling ability, such as periodically poled MgO-doped stoichiometric lithium tantalate (PPMgSLT) [7–9], have a lower nonlinear coefficient and are less efficient at generating second harmonic light as a consequence.

A highly efficient scheme for power scaling single-pass SHG is the so-called cascade of nonlinear crystals [10–14]. In a cascade of nonlinear crystals, fundamental light is focused

#239674 - $15.00 USD Received 24 Apr 2015; revised 29 May 2015; accepted 31 May 2015; published 8 Jun 2015

into a first crystal and the generated second harmonic light is kept co-propagating with the fundamental beam as both beams are re-focused into a second crystal and, potentially, more crystals thereafter. This concept is shown in Fig. 1. The contributions to the SH electric field of the two crystals can, with suitable control of the relative phase offset between the fundamental and SHG beams, be brought to interfere constructively. For the case of two identical crystals, a two-crystal cascade theoretically exhibits up to a factor 4 enhancement of the SH power compared to the output of one crystal in the limit of negligible fundamental beam depletion, see details in Section 2.1.

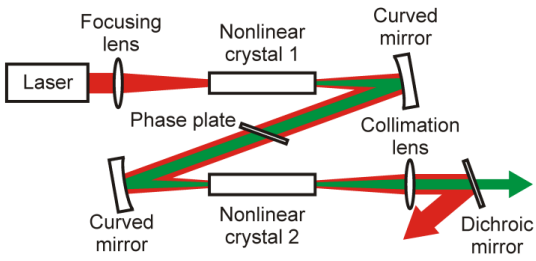

Fig. 1. Sketch of the cascade concept. The fundamental beam is shown with red, and the SH beam with green. Nonlinear crystal 1 is chosen for high efficiency, while nonlinear crystal 2 is chosen for SH power handling ability. With additional crystals, refocusing optics and phase plates, the concept can be extended to include more stages.

Fluck and Günter [10] were the first to demonstrate cascaded SHG in 1998. They used $KNbO_3$ crystals to generate 491 nm light with low-power nonlinear efficiencies of 2.4%/W in a two-crystal cascade and 3.5%/W in a three-crystal cascade. They also generated 429 nm light at 3.1%/W in a two-crystal cascade. In 2011, using PPMgSLT crystals and a fiber laser emitting up to 30 W of diffraction-limited fundamental light, Kumar *et al.* [11] showed generation of up to 13 W of green light at 532 nm in a cascade of two PPLT crystals at an efficiency of 52%. They achieved low-power nonlinear efficiencies of 5%/W and 7.8%/W in two- and three-crystal cascades, respectively. Thompson *et al.* [12] achieved 5.6%/W when doubling to 780 nm in two PPLN crystals, also with a Gaussian fundamental beam. Such cascaded setups are, in general, quite successful at achieving high nonlinear efficiencies, so properties such as thermal handling quickly become parameters of critical importance in such setups.

The concept that we demonstrate in this paper as a solution to this problem combines the high efficiency of one crystal type with the power handling ability of another crystal type. In a cascade, the first crystal generates only a fraction of the final output power and its crystal material can thus be chosen among types that do not necessarily handle high SH powers well. The materials of the subsequent crystals do have to handle high SH powers well, but a low nonlinear coefficient is more acceptable here because it is offset by the inherent enhancement factor of the cascade.

We show in this paper a comparison of two different two-crystal cascade configurations. In configuration 1, the cascade consists of two PPMgCLN crystals while in configuration 2, the first crystal is PPMgCLN and the second is PPMgSLT. Thermal effects for both configurations are studied and compared. We demonstrate that combining different crystal types proves particularly advantageous at intermediate input powers (for SHG of 1063 nm light, up to ~10 W), yielding a high nonlinear efficiency while avoiding thermal dephasing. We simultaneously demonstrate the importance of adjusting the phase delay between the crystals in a simple configuration.

The laser source used for this demonstration is a tapered diode laser that emits non-diffraction-limited light [15]. While the beam profile in the vertical direction (fast axis) is nearly Gaussian, the second moment beam propagation ratio in the horizontal direction (slow axis) is $M_x^2 = 7.7$. Despite the non-Gaussian fundamental beam, a nonlinear beam cleanup

#239674 - $15.00 USD Received 24 Apr 2015; revised 29 May 2015; accepted 31 May 2015; published 8 Jun 2015

effect nonetheless ensures that the SH light has a low second moment beam propagation ratio along both axes ($M_x^2 = 1.3$). Such a non-diffraction-limited fundamental beam is frequency doubled less efficiently than a Gaussian beam of the same power, which emphasizes the need for crystals with a high nonlinear coefficient for frequency doubling non-Gaussian laser sources.

Previously, diode lasers of this type were used to generate 1.5 W and 1.8 W of green light in single-pass, single-crystal SHG [16–18]. These results comprised the highest SHG powers from diode lasers prior to this work.

The specific case of highly efficient SHG of green light demonstrated in this article is itself relevant for multiple applications, one of which is pumping titanium sapphire lasers. Uses of titanium sapphire lasers such as the emerging field of single-source multimodal bioimaging [19,20] place high demands on the power of the titanium sapphire laser and, in turn, the power of its pump source.

2. Theory and simulations

The theory of SHG in a cascade of nonlinear crystals was originally outlined by Fluck and Günter [10]. As in their paper, we will only consider the theory in the limit of negligible fundamental beam depletion, in which the nonlinear interaction changes neither the magnitude nor the phase of the fundamental beam. We will consider the electric field in arbitrary units and approximate the phase matching condition by that of an infinite plane wave, which is sufficient to describe the general behavior of the system. For the power scaling, however, the scaling law for a focused beam is used [21].

Denoting the input fundamental beam power P_ω and the output SH power $P_{2\omega}$, we define the nonlinear efficiency η of an SHG system as the low-depletion conversion factor according to $P_{2\omega} = \eta P_\omega^2$. In order to show general trends in the results section, we will show fits to the expression for SH power output of a frequency doubled infinite plane wave that takes depletion into account,

$$P_{2\omega} = P_\omega \tanh^2 \sqrt{\eta P_\omega}. \tag{1}$$

Note that this expression is not strictly valid for focused beams if the degree of depletion approaches unity, and also that it does not take into account thermal effects, but it will nevertheless yield the correct low-power value of η and is very helpful as a guide to the eye.

2.1 Cascade power scaling law

Let $E_{2\omega}^{(j)}$ denote the complex electric field amplitude contribution to the SH field generated in the j^{th} crystal of an N-crystal cascade. By the superposition principle, the SH field after all N crystals is then simply the sum,

$$E_{2\omega} = \sum_{j=1}^{N} E_{2\omega}^{(j)}, \tag{2}$$

where phase is included through the complex addition.

When propagating from one crystal to the next, a relative phase offset between the fundamental and SH beams occurs because of the dispersion of air and the optics. In addition, for quasi-phase-matched periodically poled media, the initial and final poling domains of each crystal are generally of an unknown length due to cutting and polishing during production, thus the dispersion of the final poling domain of the j^{th} crystal and the initial poling domain of the $(j + 1)^{\text{th}}$ crystal also contribute to the phase offset. Experimentally, a phase plate is positioned between each pair of crystals which allows fine adjustment of the relative phase offset over several times 2π to achieve constructive or destructive interference, or anything in between.

#239674 - $15.00 USD Received 24 Apr 2015; revised 29 May 2015; accepted 31 May 2015; published 8 Jun 2015

If we now consider the case where the SH field contributions are individually at optimal phase matching and additionally have relative phase offsets optimized for maximum constructive interference, we can write

$$E_{2\omega}^{(j)} = \sqrt{\bar{\eta}_j L_j} P_\omega, \tag{3}$$

so that

$$E_{2\omega} = \sum_{j=1}^{N} \sqrt{\bar{\eta}_j L_j} P_\omega, \tag{4}$$

where we denote for the j^{th} crystal the nonlinear efficiency per unit length $\bar{\eta}_j$ and the length L_j.

Since the power is proportional to the squared norm of the electric field, we get for $\boldsymbol{N}$ identical crystals

$$P_{2\omega} = \left(\sum_{j=1}^{N} \sqrt{\bar{\eta} L} P_\omega \right)^2 = \bar{\eta} L N^2 P_\omega^2, \tag{5}$$

from which the basic scaling law of the cascade is apparent. As in the case of a focused beam in a single crystal, the output power is still linear in crystal length. However, a factor of N^2 introduces an enhancement factor of 4 for a two-crystal cascade, 9 for a three-crystal cascade and so on.

2.2 Generalized low-depletion theory

We will now write out the generalized low-depletion expressions for the electric field contributions $E_{2\omega}^{(j)}$ from each crystal as a function of the phase mismatches Δk_j within each crystal and the relative phase offsets ϕ_j between the fundamental and the SH fields accumulated between the j^{th} crystal and the $(j + 1)^{\text{th}}$ crystal. We regard the complex magnitudes $E_{2\omega}^{(j)}$ as phasors that are added in a phasor diagram.

By simple integration of phasor components, the complex electric field generated by crystal 1 can be written as

$$E_{2\omega}^{(1)} = \begin{cases} P_\omega \sqrt{\eta_1}, & \Delta k_1 = 0 \\ P_\omega \sqrt{\eta_1} \dfrac{e^{i\Delta k_1 L_1} - 1}{i \Delta k_1 L_1}, & \Delta k_1 \neq 0 \end{cases} \tag{6}$$

Here, the first slice of the first crystal is arbitrarily chosen to generate SH field with phase 0 (the phasor points in the positive real direction), which results in the final slice of the first crystal generating SH field with a phase equal to $\Delta k_1 L_1$. The first slice of the second crystal then generates a SH field with a phase equal to $\Delta k_1 L_1 + \phi_1$, where ϕ_1 is the relative phase offset described above, adjustable by rotating a phase plate. We can write the electric field generated in the second crystal:

$$E_{2\omega}^{(2)} = \begin{cases} P_\omega \sqrt{\eta_2} e^{i(\Delta k_1 L_1 + \phi_1)}, & \Delta k_2 = 0 \\ P_\omega \sqrt{\eta_2} \dfrac{e^{i\Delta k_2 L_2} - 1}{i \Delta k_2 L_2} e^{i(\Delta k_1 L_1 + \phi_1)}, & \Delta k_2 \neq 0 \end{cases} \tag{7}$$

More generally, we have for the j^{th} crystal ($j > 1$):

#239674 - $15.00 USD Received 24 Apr 2015; revised 29 May 2015; accepted 31 May 2015; published 8 Jun 2015

$$E_{2\omega}^{(j)} = \begin{cases} P_\omega \sqrt{\eta_j}\, e^{i\sum_{n=1}^{j-1}(\Delta k_n L_n + \phi_n)}, & \Delta k_j = 0 \\ P_\omega \sqrt{\eta_j}\, \dfrac{e^{i\Delta k_j L_j} - 1}{i\Delta k_j L_j} e^{i\sum_{n=1}^{j-1}(\Delta k_n L_n + \phi_n)}, & \Delta k_j \neq 0 \end{cases} \tag{8}$$

The total electric field is the sum of the contributions, and the power is the squared norm,

$$P_{2\omega} = \left| \sum_{j=1}^{N} E_{2\omega}^{(j)} \right|^2 . \tag{9}$$

Throughout the rest of this article, we regard only the two-crystal cascade ($N = 2$). Video illustrations that show the theoretical output power for $N = 2$ as a function of the two temperatures and the relative phase offset can be found in Media 1 and Media 2. Single-frame excerpts from these videos are shown in Fig. 2. In the simulations, experimentally measured efficiencies are used for η_1 and η_2. Experimentally measured phase matching temperature widths and center temperatures are used to determine ΔkL as a function of temperature for each crystal.

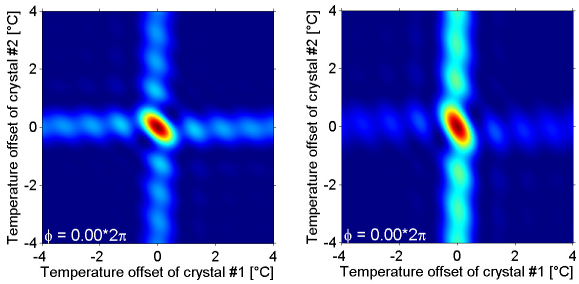

Fig. 2. Single-frame excerpts from video illustrations which show the normalized $N = 2$ cascade output power as a function of the two temperatures and the relative phase offset. **Left:** Configuration 1, where $\eta_1 = \eta_2$ (Media 1). **Right:** Configuration 2, where $\eta_2 = 0.29 \times \eta_1$ (Media 2).

2.3 Compensating for non-zero relative phase offset

It is interesting to consider the hypothetical case of a two-crystal cascade with a poorly optimized phase plate or, indeed, a setup that omits the phase plate entirely and has no other means of adjusting dispersion. We can calculate the maximum enhancement that is possible to achieve in such setups only by optimizing the crystal temperatures (phase mismatches), for any given value of the relative phase offset ϕ. We define the low-depletion cascade enhancement

$$\kappa(\Delta k_1 L_1, \Delta k_2 L_2, \phi) = \frac{P_{2\omega}(\Delta k_1 L_1, \Delta k_2 L_2, \phi)}{P_\omega^2 \eta_1}, \tag{10}$$

where $P_{2\omega}$ is the SH power output from the cascade, and $P_\omega^2 \eta_1$ is the maximum SH power output from only the first crystal in a single crystal setup. We define then the temperature-optimized enhancement

$$\kappa_m(\phi) = \kappa((\Delta k_1 L_1)_m, (\Delta k_2 L_2)_m, \phi) \tag{11}$$

as the maximum value of κ at the given ϕ. κ_m and $(\Delta kL)_m$ are calculated as a function of ϕ for two cases in Fig. 3.

#239674 - $15.00 USD Received 24 Apr 2015; revised 29 May 2015; accepted 31 May 2015; published 8 Jun 2015

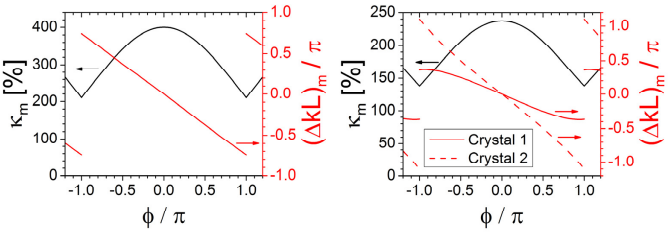

Fig. 3. Simulated temperature-optimized enhancement factor and the optimal ΔkL values as a function of relative phase offset in a two-crystal cascade. **Left**: Two identical crystals, $\eta_1 = \eta_2$, as in cascade configuration 1. In this case, $(\Delta k_1 L_1)_m = (\Delta k_2 L_2)_m$. **Right**: The case where $\eta_2 = 0.29 \times \eta_1$, as in cascade configuration 2.

In Fig. 3, the ideal case of $\phi/\pi = 0$ follows the equations of Section 2.1, with 400% and 234% enhancement in configurations 1 and 2, respectively. We see that even if the phase plate is set to the worst possible position, $\phi/\pi = \pm 1$, theory predicts that it is still possible to compensate with the crystal temperatures to obtain 210% and 138% enhancement in configurations 1 and 2, respectively. Even in these worst-case scenarios, the cascade can yield in both cases a higher power than the sum of the powers achievable with each crystal individually (200% and 129% in configurations 1 and 2, respectively).

3. Setup and results

3.1 Setup

The setup is conceptually sketched in Fig. 1. The laser is a Distributed-Bragg-Reflector tapered diode laser mounted *p*-side up and with two separate electrical contacts [15]. Operating at a wavelength of 1063 nm, it emits about 10.5 W of light with a beam that is Gaussian along the vertical axis but non-diffraction-limited along the horizontal axis. The line width of the single-frequency emission is < 6 pm, which is well within the acceptance bandwidth of the crystals used in this work. The astigmatic emission from the diode is collimated and made stigmatic and circular using an aspheric lens of focal length f = 8 mm followed by a cylinder lens of focal length f = 80 mm.

With these collimation optics, the beam propagation ratio in the horizontal axis is $M_x^2 = 7.7$, measured using a Spiricon M^2-200s profiler based on second order moments, as specified in the ISO11146 standard. This measurement method is used throughout the article. In a focus, the beam forms a circular central lobe in the intensity profile containing the majority of the power. The remaining power is distributed among minor side lobes in the horizontal direction, as can be seen in Fig. 4.

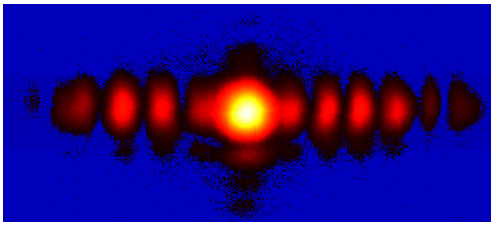

Fig. 4. The beam profile of the infrared fundamental beam in focus. A central lobe carries the majority of the power. The structure in the vertical direction (fast axis) is very slight, whereas the structure in the horizontal direction (slow axis) is more significant.

After collimation, the beam passes through a half-wave plate and an optical isolator to protect the diode from feedback and preserve the good spectral characteristics [15]. By rotating the half-wave plate, the power transmitted through the optical isolator can be varied

#239674 - $15.00 USD Received 24 Apr 2015; revised 29 May 2015; accepted 31 May 2015; published 8 Jun 2015

up to a maximal transmitted power of 9.5 W. After the optical isolator, another half-wave plate rotates the polarization to vertical. The light is then incident on a pair of steering mirrors, after which it is focused into the first crystal with a spherical lens of focal length f = 150 mm. The crystal is installed into a temperature-controlled closed-top oven, and the central lobe beam waist inside the crystal is measured to be 85 μm in diameter (focusing parameter $\xi = 1.9$). This focusing condition was chosen because it was experimentally determined to be optimal at our highest input power.

The diverging laser beams exiting the first crystal are incident in an angle of 6° on a spherical concave mirror with radius of curvature R = 200 mm. This mirror is high-reflective coated for both 1063 nm and 532 nm and achromatically collimates the beams. On the diagonal stretch, the beams pass through a phase plate mounted on a rotation stage. This phase plate is simply an uncoated BK-7 glass window of thickness 3 mm oriented at Brewster's angle relative to the vertically polarized beams. While the phase plate is mounted such that it is tilted around the lateral axis to get to Brewster's angle, adjustment of the phase offset is done by rotating with a rotation stage around the vertical axis. The relative difference in vertical displacement of the two beams is negligible, on the order of 1% of the collimated beam width.

From here, the two co-propagating beams are re-focused using another curved mirror identical to the previous one into the next crystal, forming a focus of the same size as in the first crystal. This crystal is also mounted in a temperature-controlled closed-top oven. Finally, a dichroic mirror separates the fundamental and second harmonic beams.

To illustrate the necessity of good power handling ability in the second crystal, we compare two different crystal configurations. In configuration 1, both crystals are PPMgCLN crystals of length 50 mm. In configuration 2, the first is a PPMgCLN crystal of length 40 mm and the second is a PPMgSLT crystal of length 35 mm. The choice of crystal lengths was limited by availability.

3.2 Power dependence

3.2.1 Single-crystal SHG characterization

In Fig. 5, power curves of the three types of crystals used are shown, as measured in a standard single-crystal setup. Input power was varied by turning the half-wave plate before the optical isolator. For each input power, the temperature set point of the crystal mount was reoptimized. The difference between the two PPMgCLN crystals is quite small and both show a deviation from the fit at high power, probably the onset of slight thermal dephasing due to localized heating caused by SH absorption. Other authors have observed and modelled similar thermal effects in lithium tantalate, occurring at higher powers [22]. The PPMgSLT crystal shows a lower efficiency, as expected, but no deviation from the fit for these powers.

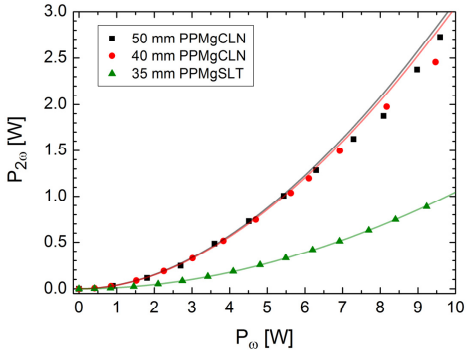

Fig. 5. SH power curves for the three types of crystals used. Temperature set point was reoptimized at each point. Fits to the expression for depleted SHG are shown. For the PPMgCLN crystals, only points below 4 W input power were included in the fits.

#239674 - $15.00 USD Received 24 Apr 2015; revised 29 May 2015; accepted 31 May 2015; published 8 Jun 2015

Low-power nonlinear efficiencies and maximum SH powers are shown in Table 1, along with the temperature set point shifts required for optimal SHG at maximum power.

Table 1. Single-Crystal SHG Characterization

	η [%/W]	$P_{2\omega}$ [W]	ΔT [°C]
50 mm PPMgCLN	4.0	2.7	–0.50
40 mm PPMgCLN	3.9	2.5	–0.65
35 mm PPMgSLT	1.1	0.89	–0.05

[a]Showing low-power nonlinear efficiency, maximum SH power and the temperature set point shift required to retain optimal SHG.

The reason that the 50 mm crystal required less of a temperature shift than the 40 mm crystal may be a slight difference in thermal contacting between crystal and mount as well as slight differences in crystal purity, as they were produced in different batches.

3.2.2 Cascade configuration 1

In configuration 1 with 9.5 W input power, the first crystal yields 2.75 W of green power, with the addition of the second crystal raising this to only 3.6 W, with drastic phase matching hysteresis and instability also observed in lithium niobate by other authors [5]. The beam profile shows power-dependent circular structure (see Fig. 6(a)), fluctuating irregularly on a time scale of approximately half a second. Both wave-front distortions and power fluctuations were apparent. This is consistent with thermal dephasing caused by absorption of the SH light. Due to the strong phase matching instabilities, it was not possible to map out a meaningful power curve for the cascade in configuration 1. The nonlinear efficiency at low powers was high, however, at 11.5%/W. No indications of long-term damage such as photorefractive distortion were apparent.

3.2.3 Cascade configuration 2

In contrast to configuration 1, the cascade in configuration 2 reaches up to 3.72 W at a fundamental input power of 9.5 W, despite the lower efficiencies of both crystals when measured in the low-power regime. No phase matching instability is observed using configuration 2, and the far field beam profile is nearly Gaussian, as seen in Fig. 6(b). This is consistent with the expectation that lithium tantalate exhibits less pronounced thermal effects than lithium niobate.

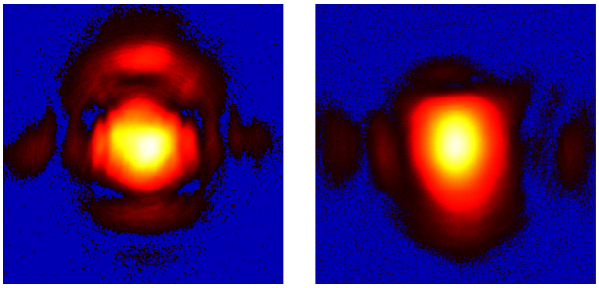

Fig. 6. Far field intensity profile of SH cascade output at maximum SH power. **Left**: Configuration 1. Significant circular distortion appears at high SH power (3.6 W). **Right**: Configuration 2. Beam is diffraction limited even at the highest SH power (3.7 W).

The SH output power of the cascade in configuration 2 is shown in Fig. 7, along with a fit to the expression for depleted SHG. The fit yields $\eta = 6.7\%/\mathrm{W}$. The deviation from the fit for high powers is likely caused by the onset of slight thermal effects in the lithium niobate crystal, as is evident in Fig. 5. As in the case of configuration 1, no indications of long-term damage such as photorefractive distortion were apparent. The maximum power achieved, 3.72 W, is to date the highest power achieved by frequency doubling of a diode laser. The

#239674 - $15.00 USD Received 24 Apr 2015; revised 29 May 2015; accepted 31 May 2015; published 8 Jun 2015

opto-optical conversion efficiency is 39% and the wall-plug electro-optical efficiency is 9.6%. These results are obtained in spite of the non-Gaussian beam profile of the fundamental beam, with an $M_x^2 = 7.7$ of the input while achieving $M_x^2 = 1.25$ of the SH output. This nonlinear beam cleanup effect is consistent with previous results on SHG of tapered diode lasers [16].

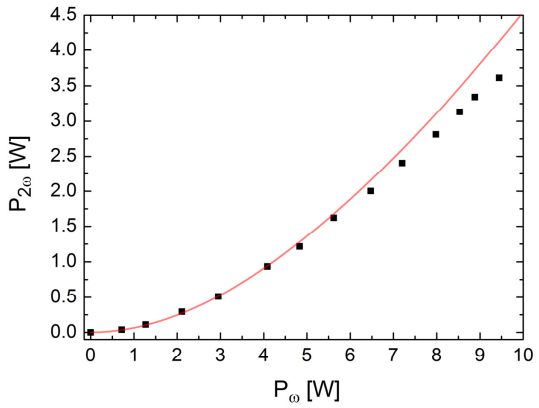

Fig. 7. SH power curve of the cascade in configuration 2. Temperature set points were reoptimized for each point. A fit is shown to the expression for depleted SHG, resulting in η = 6.7%/W . Only the points below 4.5 W input power were included in the fit.

3.3 Phase offset dependence

When the phase plate is rotated around the vertical axis by an angle θ, it introduces a change in the relative phase offset ϕ of the two wavelengths. By using the Sellmeier equations for BK-7 glass [23], Snell's law and some geometric calculations, this relative phase offset $\phi(\theta)$ is simple to calculate. Based on the cascade enhancement κ defined in Section 2.1, we define the phase matched cascade enhancement $\kappa_0(\phi) = \kappa(0,0,\phi)$, which is the enhancement achieved while both crystal temperatures remain at the values optimal for individual phase matching.

3.3.1 Cascade configuration 1

In Fig. 8, experiment and theory is compared for crystal configuration 1. This was done at low power to avoid the severe thermal dephasing typical of configuration 1. The dashed line indicates the theoretical maximal value of κ_0 (400%) assuming no losses and perfectly compensated relative phase offset. The solid curve shows the theoretical dependence of κ_0, normalized to the achieved maximum value (361%) and taking Fresnel losses at the phase plate into account. The arbitrary relative phase offset at $\theta = 0°$ was the only free fitting parameter. The lowest value of κ_0 is 4%, corresponding to 96% of the green light generated in the first crystal having been back-converted to infrared in the second crystal.

#239674 - $15.00 USD Received 24 Apr 2015; revised 29 May 2015; accepted 31 May 2015; published 8 Jun 2015

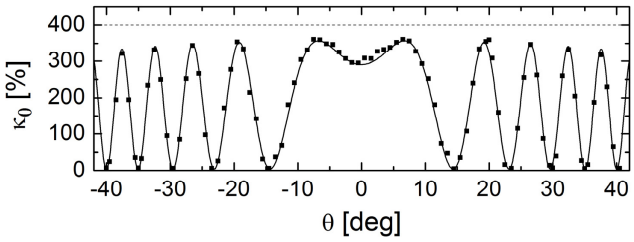

Fig. 8. Phase matched cascade enhancement κ_0 as a function of rotation angle of the phase plate around the vertical axis. Configuration 1, low power. Dashed line: theoretical maximum. Points: measurements. Solid curve: Theory normalized to the achieved maximum enhancement.

3.3.2 Cascade configuration 2

The same comparison for configuration 2 at low power is shown in Fig. 9. Based on the experimental measurement of the respective effective nonlinear efficiencies of the two crystals, the theoretical maximal value of κ_0 is 234%, and the theoretical minimal value is 21%. Experimentally, enhancements from 30% up to 204% were achieved, in fine agreement with expected values.

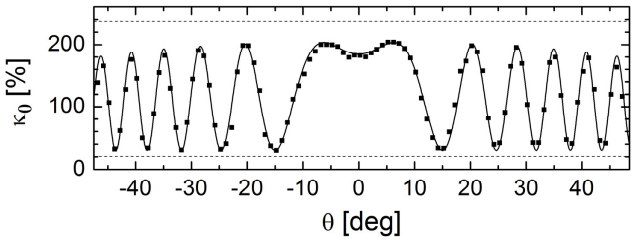

Fig. 9. Phase matched cascade enhancement κ_0 as a function of rotation angle of the phase plate around the vertical axis. Configuration 2, low power. Dashed lines: theoretically maximal and minimal κ. Points: measurements. Solid curve: theory normalized to the achieved maximum and minimum.

For configuration 2, the scan at high power (9.5 W input) is shown in Fig. 10. High fundamental beam depletion is apparent. Due to the strong phase matching instabilities, it was not possible to measure a meaningful phase offset scan for configuration 1 at high power.

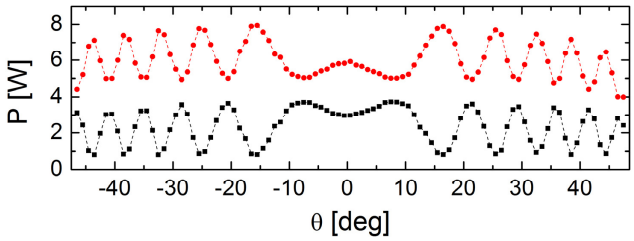

Fig. 10. SH (red circles) and fundamental (black squares) output of the cascade in configuration 2 at high power, as a function of rotation angle of the phase plate around the vertical axis. Strong fundamental beam depletion is observed.

#239674 - $15.00 USD Received 24 Apr 2015; revised 29 May 2015; accepted 31 May 2015; published 8 Jun 2015

3.4 Temperature dependence

Using configuration 2, we also made measurements in which the temperatures of the two crystals were varied while the position of the phase plate was held constant. This was done at low power for two phase plate settings: constructive interference and destructive interference. Furthermore, a scan at high power was performed at constructive interference. These results are shown with comparison to the theory in Fig. 11. Good qualitative agreement with the theory is seen. More complex structure appears at high power, presumably due to thermal effects in the first crystal. These effects do not significantly impact the maximum power achievable in configuration 2, but simply suggest that we are operating PPMgCLN just below the limit of stable performance in our setup.

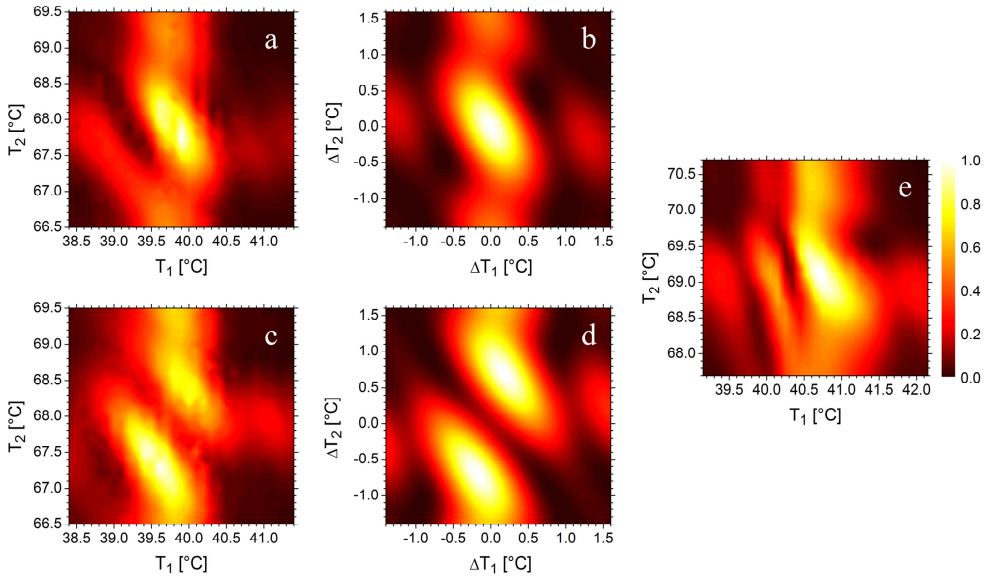

Fig. 11. Normalized output power from configuration 2 as a function of temperature set points of the two crystals, for various powers and phase plate settings. Linear interpolation is used between measurement points. The color scale shown in **e** applies to all plots. **a**: Low power measurement roughly at constructive interference. **b**: Simulation with $\phi = 0$. **c**: Low power measurements roughly at destructive interference. **d**: Simulation with $\phi = \pi$. **e**: Measurement at maximum input power and constructive interference.

3.5 Beam quality

An example of the focus beam profile of the fundamental laser light is shown in Fig. 4. Since the fundamental beam is non-Gaussian, the position dependence of the fundamental beam depletion is of great interest. One very useful figure of merit is the power in the central lobe P_{CL} of the focused beam profile.

We carried out four focus beam profile measurements of the infrared and SH beams exiting the second crystal of the cascade in configuration 2. One without any crystals phase matched, one with each crystal phase matched and one with both crystals phase matched with the phase plate optimized for maximum output. The results are listed in order of increasing fundamental beam depletion in Table 2.

#239674 - $15.00 USD Received 24 Apr 2015; revised 29 May 2015; accepted 31 May 2015; published 8 Jun 2015

Table 2. Beam Quality Parameters for Various Degrees of Depletion

Phase matched crystals	P_{CL} / P		M_x^2		M_y^2	
	Fund.	SH	Fund.	SH	Fund.	SH
None	67.3%	-	7.68	-	1.43	-
Only #2	64.6%	>99%	8.09	1.14	1.44	1.04
Only #1	62.4%	>99%	7.69	1.15	1.49	1.14
#1 and #2	54.7%	>98%	9.91	1.25	1.50	1.13

[a]Fractional powers in central lobe of the focus beam profiles and beam propagation ratio in the horizontal and vertical directions of the residual fundamental and the SH light, for various combinations of crystals at phase matching (configuration 2). In all cases, the beams were measured after passage of both crystals. The rows are arranged in order of increasing fundamental depletion, since crystal #2 (PPMgSLT) is less efficient than crystal #1 (PPMgCLN).

As one might expect, the relative power in the central lobe of the fundamental beam drops off as the depletion of the beam increases. The tendency for fundamental residual M_x^2 to rise with increasing depletion is also consistent with the majority of conversion happening in the central lobe (see Fig. 4), leaving the side lobes to be more strongly represented in the residual beam.

As a result of this, one expects a slightly increased relative degree of conversion of the side lobes as the depletion increases, which explains the increase of SH M_x^2. Also in the vertical direction, both the SH and fundamental M_y^2 are expected to rise slightly with increasing depletion based simply on the expected behavior for Gaussian beams [24].

Because, at optimal SH generation, the total fundamental power decreases from 9.5 W before the first crystal to 5.0 W after the second crystal, we can calculate that the absolute power in the central lobe decreases by 57% when the beam goes through the system, while the absolute power outside the central lobe decreases by 27%.

4. Discussion and conclusions

In the comparison of the two configurations, it is evident that periodically poled MgO-doped congruent lithium niobate is inadequate for power scaling second harmonic generation above roughly 3 W with enough stability for a practically feasible system. Although 3.6 W of SH light could be generated with two PPMgCLN crystals, strong phase matching instabilities in these crystals lead to a distorted SH beam profile, lowered overall efficiency and erratic fluctuations in output power. These are probably all manifestations of strong thermal dephasing, as other authors have also observed [5]. For any practical purpose, such deteriorate behavior renders this configuration of limited use.

On the other hand, the second crystal configuration, in which a periodically poled MgO-doped congruent lithium niobate crystal was followed by a periodically poled stoichiometric MgO-doped lithium tantalate crystal, showed negligible thermal effects and actually generated a higher SH output, 3.7 W, despite the fact that lithium tantalate possesses a lower nonlinear coefficient than lithium niobate, and additionally despite the fact that both crystals were shorter than in configuration 1. The SH output showed no distortion and was diffraction limited, despite the non-Gaussian input fundamental light. This configuration would indeed be applicable for power scaling purposes for practical use, e.g., in multimodal bioimaging applications [19,20].

While adding additional crystals to the setup would in general raise the efficiency even further, it would in our specific case also lead to a slightly worse beam profile due to the increased depletion of the non-Gaussian fundamental beam. To keep our output beam diffraction-limited, we chose not to add more crystals to our cascade.

#239674 - $15.00 USD Received 24 Apr 2015; revised 29 May 2015; accepted 31 May 2015; published 8 Jun 2015

The 3.72 W of second harmonic light generated in this work constitutes, at the time of writing, a new world record of power generated in frequency doubling of diode lasers. The high opto-optical conversion efficiency of 39% was achieved despite the non-Gaussian input fundamental beam. By suitable choice of crystal material, the cascade concept can thus successfully combine a high nonlinear coefficient in the first crystal with good power handling properties of subsequent crystals. Adjustment of the phase delay between the fundamental and SH beams with the use of a rotatable transparent window at Brewster's angle proved to be a very useful and simple scheme.

Only two-crystal cascades were studied in this work, but more crystals can easily be added to power scale further. The favorable N^2 scaling law in the low-depletion limit is especially advantageous in applications at significantly different wavelengths where less efficient crystal materials must be used, and where the fundamental powers may be lower. With proper choice of nonlinear materials, cascaded second harmonic generation is a highly applicable and practical concept for power scaling.

Acknowledgments

European Union FP7 ICT project FAMOS (317744).

#239674 - $15.00 USD Received 24 Apr 2015; revised 29 May 2015; accepted 31 May 2015; published 8 Jun 2015